SenseORAN: O-RAN based Radar Detection in the CBRS Band

Guillem Reus-Muns, Pratheek S. Upadhyaya, *Student Member, IEEE*, Utku Demir, *Member, IEEE*, Nathan Stephenson, Nasim Soltani, *Student Member, IEEE*, Vijay K. Shah, *Member, IEEE*, and Kaushik R. Chowdhury, *Senior Member, IEEE*

Abstract*—Open RAN (O-RAN) has the potential for revolutionizing not only cellular communication but also spectrum sensing by carefully controlling uplink/downlink traffic in shared spectrum bands. In this paper, we present the design of *SenseORAN*, which detects the presence of radar pulses within the Citizens Broadband Radio Service (CBRS) band. SenseORAN is especially useful for scenarios where these pulses (highest priority) are fully overlapping with interfering LTE signals (secondary priority licensee), requiring immediate detection of such an occurrence. This design paradigm of re-using existing cellular infrastructure with ORAN-compliant sensing and communication slices can potentially eliminate the need for dedicated spectrum sensors along the coastline as well as severe restrictions on the transmit power for the LTE operators that are enforced today. Our approach involves a machine learning module deployed as a *Radar Detection xApp* at the near-Real-Time (near-RT) Radio Access Network (RAN) Intelligent Controller, i.e., near-RT RIC. The base station or gNB (i) uses the you-only-look-once (YOLO)-based machine learning framework that is modified to detect radar signals present within spectrograms generated from I/Q samples collected during the regular uplink cellular operation, and (ii) maintains a list of 'occupied' channels in the $3.5\,\mathrm{GHz}$ CBRS band that indicate radar presence. Our design is validated with (i) an over the air collected dataset composed of Type 1 radar and standard-compliant LTE waveforms, and (ii) an experimental testbed of SDRs running a complete Open RAN stack with a near-RT RIC implementation integrated with our YOLO-based xApp. We show radar detection accuracy of 100% under SINR conditions $\geq 12\,\mathrm{dB}$ after combining 7 spectrograms into a single decision. Furthermore, using testbed results, we demonstrate that the gNB can be reconfigured to avoid radar interference within $866\,\mathrm{ms}$, which represents a reduction of 85.5% over the $60\,\mathrm{s}$ response time mandated for pausing cellular operation in detecting radar presence in the CBRS band today.

***Index Terms*—CBRS, Radar detection, O-RAN, AI, xApp**

Manuscript received 7 January 2023; revised 2 June 2023; accepted 2 August 2023. This work was supported by the U.S. National Science Foundation (NSF) grants CNS 2112471, CNS 2229444, and CCRI 2120411 along with the Roux Institute and Harold Alfond Foundation. (*Corresponding author: Guillem Reus-Muns.*)

Guillem Reus-Muns, Utku Demir, Nasim Soltani, and Kaushik Chowdhury are with the Institute for the Wireless Internet of Things, Northeastern University, Boston, MA 02120 USA (e-mail: greusmuns@ece.neu.edu; u.demir@northeastern.edu; soltani.n@northeastern.edu; krc@ece.neu.edu).

Pratheek S. Upadhyaya is with the Department of Electrical and Computer Engineering, Virginia Tech, Blacksburg, VA 24061 USA (e-mail: pratheek@vt.edu).

Nathan Stephenson and Vijay K. Shah are with NextG Lab@GMU, George Mason University, Fairfax, VA 22030 USA (e-mail: nstephe7@gmu.edu; vshah22@gmu.edu).

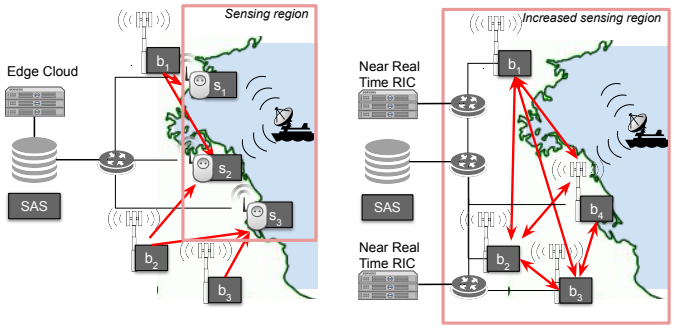

(a) CBRS design today with sensors s_1, s_2, s_3 reporting to SAS.

(b) Open RAN-based CBRS with sensing only by BS b_1, b_2, b_3, b_4.

Fig. 1: Currently, ESC sensors s_1, s_2, s_3 detect radar in the CBRS band in (a), which may be subject to interference from cellular BSs b_1, b_2, b_3 shown by red arrows. The data from ESC sensors is reported to the SAS. In the proposed architecture in (b), the b_1, b_2, b_3 are O-RAN compliant BSs, which use machine learning based *xApp*s in the near-RT RICs to accurately detect radar and for optimal BS reconfiguration upon detected radars. This increases the sensing region and reduces deployment overhead by re-using existing cellular infrastructure.

I. Introduction

The scarcity of wireless spectrum has spurred interest in spectrum sharing within federal bands, provided that the priorities of the incumbents are protected. The CBRS band in the 3.55-3.7 GHz frequency range is an illustrative example of this shared-spectrum paradigm, where 4G LTE and 5G operators (also called as Priority Access License or PAL users) and unlicenced users (General Authorized Access or GAA users) may coexist along with the higher priority naval radar. CBRS defines a central entity, called SAS, that requires PAL and GAA users to register and assigns medium access according to the tiered priority scheme. Incumbent and PAL users are protected from the GAA interference, but no interference protection is guaranteed for GAA users [1], as shown in Fig. 2.

Within the CBRS band today, a number of dedicated environmental sensing capability (ESC) sensors are deployed along the coast for detecting radar pulses. We propose a radically different vision in this paper, wherein we suggest eliminating the need for ESC sensors. Instead, in SenseORAN, O-RAN compliant base stations (BSs or interchangeably denoted as gNBs) perform the task of sensing, with the goal of maximizing the accuracy of radar detection while maintaining acceptable level of service for the associated clients. While we frame the problem in context of ship-borne radar detection in the CBRS band, SenseORAN is designed to be extensible in

other bands that are being considered for mixed use operation, such as the 3.1-3.5 GHz band, where the detection of mobile radar incumbent becomes a challenging problem- no longer can ESC be deployed only along the coastline (unlike CBRS). These are complex decisions, where fixed policy-based approaches do not adapt well to dynamically changing mobile radar trajectories, interference conditions, and cellular-traffic.

•**Limitations of today's CBRS architecture:** Current CBRS rules adopt a conservative approach, where cellular operators are forced to operate hundreds of kilometers away from the coast [2]. The transmission power is limited to 50 W (37 dBm/MHz) [3], such that the aggregated interference and noise power at ESCs is below $-109\,\mathrm{dBm/MHz}$ [4]. This aims to minimize interference to the ESC, as the latter must detect the radar *even when there is an active PAL user transmitting* (see Fig. 1a). While effective, such rules drastically reduce cellular coverage and connectivity in the coastal regions of the country, which also contain high population density. CBRS rules also do not specify how to detect radar pulses if they are fully overlapping within a cellular signal. ESC sensors are deployed by private companies after federal certification, which increases cost of the overall roll-out and forces judicious selection of installation locations (there are only 220 ESCs along the entire US seaboard as per data retrieved in August 2020 [5]). Finally, other spectrum bands, e.g., 3.1-3.45 GHz [6], are being considered for sharing that have incumbent radar with greater flexibility of motion, such as airborne or terrestrial radar. A limited number of ESCs cannot cover the vast geographical span needed to monitor for radar, and also wide-scale curtailing the transmission power of cellular BSs may defeat the premise of enhance connectivity through spectrum sharing. For these reasons, we propose a solution based on two transformative technologies: (i) machine learning for radar signal detection and (ii) optimizing the parameters of a programmable and O-RAN-compliant cellular network.

•**Proposed approach:** Our solution to the above problems is intuitive: we propose to shift the burden of spectrum sensing to the PAL users/cellular operators, where a gNB acts as pseudo ESC, reporting any detected radar pulses to the spectrum access system (SAS), as shown in Fig. 1b. While dense deployment of such gNBs will undoubtedly increase the sensing region, how to perform sensing effectively and reconfigure the PAL users still remains an open challenge. For this, we propose a two-stage approach involving machine learning for radar detection. *Stage I: Sensing slice*: In this stage, each gNB senses the RF spectrum of interest for a finite duration of time to create a spectrogram, which is then given as input to a trained image classification network using machine learning and implemented as an xAPP in the near-RT RIC. The use of spectrograms overcomes the privacy issues related to storing and transporting in/quadrature-phase (I/Q) samples. We show how off-the-shelf convolutional neural network (CNN) architectures, e.g., YOLOv3 [7], can be effective in detecting radar pulses, even when they fully overlap a wider LTE/5G signal and under diverse traffic conditions. *Stage II: Network reconfiguration*: In this stage, all cellular network operations are turned off such that the bands where radar is detected are excluded for future use for communication. This is compliant with the current CBRS procedures, which gives full priority to radar users.

Since these are both external approaches that are not integrated within the 5G standard, the only way to realistically deploy such forward looking strategies is to adopt programmable cellular network standards, where interfaces are *open* to hardware and software components from different vendors. For this reason, we choose the O-RAN framework [8], where both the *Stage I* YOLO and the *Stage II* BS reconfiguration are executed within *xApps*, in near-RT RICs that have access times of around 10 ms-1 s, as shown in Fig. 1b (Sec. III-B gives more O-RAN details).

•**Contributions in O-RAN based sensing for CBRS**: Incorporating sensing capabilities as part of the O-RAN architecture, while being CBRS compliant, poses several challenges. We summarize them below:

- SenseORAN's machine learning modules must be wrapped within a specific format called as an xApp, in which the time needed to collect sensed data, create spectrograms, relay them over O-RAN standardized interfaces (e.g., the E2 interface connects the PHY layer) to the near-RT RIC, execute the models and then obtain back the outcomes must be within a fraction of the permissible 60 s of reporting window allowed by the Federal Communications Commission (FCC) for classical ESC operation [4]. We characterize delays over interfaces, compute end-to-end processing times, and other O-RAN specific practical overheads that can impact latency and accuracy of our xApp decision in Sec. VIII-A.
- We minimally modify YOLOv3 to enable the model to detect embedded radar pulses within cellular signals. Specifically, our model is trained in an over-the-air (OTA) collected dataset. We consistently achieve a recall of 100% at the radar $SINR$ level of 20 dB, which is the highest allowed $SINR$ value by the FCC [9]. In fact, we obtain 100% recall at the radar $SINR$ level of as low as 12 dB under low-noise high-interference scenarios, exceeding the FCC requirement overwhelmingly. We evaluate the performance of our model over different traffic conditions, $SINR$ and INR values, and number of available spectrograms. We showcase our $SINR$ dependent evaluation in Secs. VIII-B-VIII-C.
- The CBRS band mandates that cellular systems operate in Time Division Duplexing (TDD), where both uplink (UL) and downlink (DL) share the same frequency band. Thus, given the cellular frame structure, continuous data collection for radar detection might not be possible and different sub-frames need to be appended to generate a spectrogram that is representative of the band being sensed. We discuss creating this custom-spectrogram further in Sec. VI-A.
- As shown in Fig. 1b, a single near-RT RIC may serve multiple BSs, which raises concerns of congestion on the E2 interface. We evaluate the congestion effect in Sec. VIII.
- Running radar detection as part of the O-RAN architecture in form of an *xApp* presents certain system level

challenges. We have implemented the YOLO based xApp using open source libraries (srsRAN) and real hardware (Sec. VII). We release all simulation and over-the-air datasets for radar detection, YOLOv3 model [10], and open source O-RAN implementation code [11] to the community for further research.

II. Related Work

A. Prior work on O-RAN

Polese *et al.* [12] provide detailed review of the fundamentals of O-RAN architecture, interfaces, security, algorithms, and outline future research areas. There are a number of systems level and tool development efforts that continue to benefit the research community: In [13], Upadhyaya *et al.* create a prototype testbed for O-RAN for next generation implementations using USRPs. Their implementation is based on *srsRAN* and they focus on the E2 interface, by developing two xApps for the near-RT RIC. The first xApp is an improved version of the KPIMON xApp, which collects key performance indicators and developed by the O-RAN Software Community. The second xApp is an extended version of the RAN slicing xApp by POWDER [14]. However, this work is yet to be integrated in other types of cellular deployments, such as CBRS. Bonati *et al.* [15] introduce an open and virtualized prototyping platform for next generation cellular systems, called SCOPE. SCOPE is a ready-to-use portable container that embodies various wireless deployments. SCOPE's protocol stack is based on *srsRAN*, but the authors introduce network slicing, additional MAC-layer scheduling policies, the PHY-layer parameter change capability, and a data collection module for ML/AI applications. The authors tested SCOPE on the NSF Colosseum, world's largest wireless emulator, an indoor testbed called Arena, and NSF POWDER, a community-scale testbed and part of the PAWR family of externally accessible platforms by training a Deep Q-Network agent, which is a Deep Reinforcement Learning (DRL) solution for problems with discrete actions. This agent adapts slicing and scheduling schemes at run time to maximize the network throughput.

D'Oro *et al.* [16] introduce the concept of an *rApp*, named OrchestRAN, which operates in the non-RT RIC and aims for network automation in an O-RAN setting. They formulate the problem in a tree structure, in which there is a flow of network packages and also has option to share models among the O-RAN nodes. The rApp in this work computes the optimal set of data-driven algorithms and their execution location to achieve specifications from network operators. The authors evaluate the rApp using its model sharing feature, achieved throughput, and buffer sizes.

In [17], Polese *et al.* propose an xApp for automatic control of an O-RAN based cellular network. They again use DRL to perform scheduling and network slicing, e.g. categorizing user based on their data usage, which is based on [15]. In addition to evaluating achieved throughput, they also show how online training can help pre-trained models evolve and meet the demands of the specific deployment environment.

B. Prior work on CBRS

Soltani and Chaudhary *et al.* [18] propose a new ESC sensor concept in the CBRS band, called ESC+. Their aim is to detect radar and cellular signals (authorized and unauthorized users). They feed spectrograms into a custom made neural network (NN) to detect aforementioned identities in two stages. In the first stage, signal regions are detected coarsely to focus on, because radar pulses have much smaller duration compared to cellular users. Then, a finer search is applied to detect radar signals. They achieve 100% accuracy using simulated data. Lees *et al.* [19] show that deep learning methods outperform classical methods in signal detection when they use spectrograms, by comparing 13 different methods. In the end, they demonstrate that their 3-layer NN architecture offers the best accuracy vs. computational complexity tradeoff, achieving 0.99 for the area under the curve (AUC) metric for Receiver operating characteristic (ROC) curves. Caromi *et al.* [20] propose several CNNs to detect signals in the CBRS band. They utilize raw signal magnitudes and spectrograms in their models to detect the presence and absence of radar signals. In their previous work [21], they propose detecting radar signals through Support Vector Machines (SVM), which is trained using field measurements with additional computer generated LTE and Gaussian noise signals. Sarkar *et al.* [22] propose a deep learning based real-time ESC sensor using signal spectrograms for detecting radar signals and estimating their bandwidth. Their YOLO-based method is able to detect radar signals with the accuracy of 99% in the presence of noise using SDRs. However, no prior work has studied this problem under different noise and interference ratios, as we describe in Sec. VI.

Ying*et al.* [23] propose a graph theory based formulation that will allow SAS-assisted dynamic channel assignment among PAL and GAA users in the CBRS band, by mitigating their interference towards each other. They solve their formulation via heuristic methods, which is evaluated in simulations using WiFi hotspot data, achieving 93% consistent service for GAA users. Grissa *et al.* [24] approach the channel access problem in the CBRS band from a privacy angle, by reducing the sensitive information required to share for GAA users to obtain spectrum availability information, while still abiding the FCC regulations. Their proposed framework, *TrustSAS*, makes use of cryptography and blockchain elements, by forming GAAs into clusters, where cluster leaders are responsible for overall cluster dynamics by employing multi-server private information retrieval (PIR) protocol.

C. Novelty over Prior Work

In summary, state-of-the-art CBRS work has evolved in two mutually exclusive directions i) signal detection, and ii) channel allocation for secondary users. However, a fully operational CBRS system must take both the aforementioned direction together. Also, to the best of our knowledge, except a conceptual study, where Smith *et al.* [25] propose utilizing O-RAN for spectrum sharing between 5G and government satelite systems, there is no actual implementation of CBRS band channel access in the O-RAN context. SenseORAN

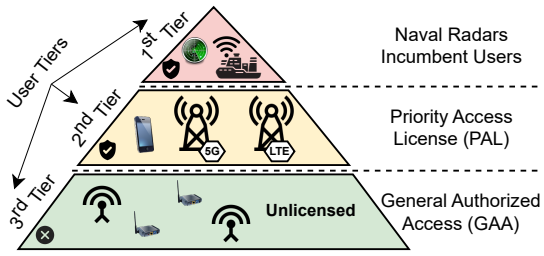

Fig. 2: CBRS tiers.

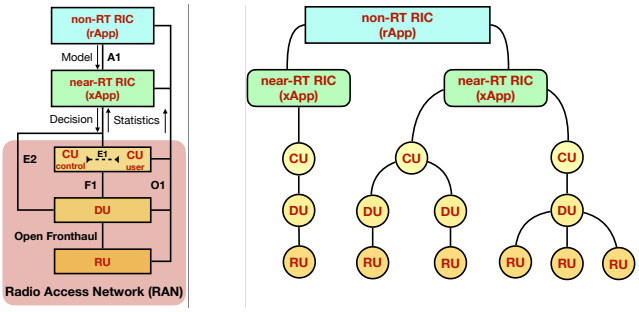

(a) O-RAN layers. (b) Connection between O-RAN layers.

Fig. 3: Basic O-RAN architecture (given in (a)) consists of RAN nodes (RU, DU, and CU), near-RT RIC and non-RT RIC, which hosts third party *xApp*s and *rApp*s, respectively. RAN nodes provide network data to the RICs, which in turn return critical network decisions through open interfaces. Higher level O-RAN components are able to control multiple lower level components (given in (b)), creating a tree-based control structure over the entire network.

distinguishes itself from prior work for CBRS via i) integrating signal detection, specifically radar, and channel allocation into one holistic study, ii) implementing the proposed idea using well known standard-compliant software that facilitates future adoption into the next generation cellular systems, i.e., O-RAN, iii) release of the dataset and models that we use in this unique study. Additionally, we propose using already available base stations for ESC sensors, and this architectural novelty not only will provide cost reduction, but also expand the radar sensing capability for aerial and terrestrial vehicular radars.

III. Motivation for O-RAN in the CBRS Band

In this section, we describe the spectrum access methodology in the CBRS band and how the O-RAN relevant architectural elements can be beneficial for radar detection in this band.

A. Current Cellular Technology in the CBRS Band

As described in Sec. I, the CBRS band presents a tiered structure (Fig. 2), where different users can access the medium with different priority levels depending on their category. In this work, we focus on the first two tiers, where radar and 5G are the incumbent and PAL users, respectively. Incumbents can access the medium with no constraints and the ESC sensors notify the SAS when they are detected in a specific band. However, relying on dedicated sensing infrastructure for radar detection requires sensors to be deployed all over the coastline. Instead, we propose to reuse the existing cellular infrastructure to also serve as sensing equipment. In particular, we aim to use existing BSs to run radar detection algorithms on top of their regular communication operations. However, such paradigm is not supported by current cellular infrastructure, which tend to be proprietary with vendor-locked black-box designs. This makes it difficult for third parties to design solutions that extend the abilities of the cellular infrastructure. To this end, we leverage O-RAN, an emerging and transformative paradigm for cellular technology that incorporates computing capabilities and open interfaces. It allows ML algorithms to run as part of the architecture and as we show in this paper, the ML models can be deployed for sensing tasks, apart from controlling network slices. In the following subsection, we briefly review O-RAN concepts and its architectural elements that are most relevant to this work.

B. O-RAN vs. Existing Cellular Technologies

O-RAN allows disaggregated design, where multiple components are interconnected through open interfaces. Additionally, O-RAN also introduces different RAN Intelligent Controllers (RICs) that reconfigure and optimize the network by leveraging data collected at multiple points across the protocol stack. This approach poses a radical change in the way cellular networks are designed, where RAN components are sold by vendors as integrated solutions. The latter typically implement every layer of the protocol stack and provide no reconfiguration opportunities to operators. All these features that O-RAN has to offer reflect into lower operational and deployment costs, also fostering agile updates, innovation, and market competitiveness [12]. Therefore, we utilize the possibility of defining custom sensing slices through O-RAN to achieve our goal of radar detection in the CBRS band. Next, we summarize the O-RAN interfaces, the node structure and the RICs that are relevant to SenseORAN.

O-RAN Nodes. O-RAN architecture, shown in Fig. 3a, extends 3GPP's 7.2 split, distributing the functionalities of the Radio Access Network (RAN) among Radio Unit (RU), Distributed Unit (DU), and Control Unit (CU), which are collectively known as RAN nodes. For further details, we refer the reader to [12].

O-RAN Interfaces. Communication and data exchange through *open* interfaces provide compatibility among network components from different vendors. This eliminates the concept of *black box*, enabling more democratic, innovative, and competitive cellular market. In this work, we focus on the E2 interface, which provides connectivity between the BS and near-RT RIC (Fig. 3a). Solutions running at the near-RT RIC are encapsulated into xApps, which are applications that support custom logic for radio resource management through standardized interfaces.

O-RAN Components. O-RAN introduces two RICs that provide management and control in the network at i) near-real-time (near-RT), with response times between $10\,\mathrm{ms}$ and $1\,\mathrm{s}$, and ii) non-real-time (non-RT), with response times $> 1\,\mathrm{s}$

(Fig. 3a). In this work, we focus on the near-RT RIC, which is where the BS reconfiguration and radar detection algorithm will run as custom-designed xApps. As mentioned previously, the near-RT is connected to the BS through the E2 interface, which will be used to share spectrogram information at the near-RT RIC and reconfigure the BS if a radar transmitter is present.

C. O-RAN in the CBRS band

As mentioned earlier, regular 4G/5G cellular infrastructure does not support radar detection, or running intelligence in general, as part of an already existing deployment. Nevertheless, radar detection is a tempting service opportunity for cellular operators, as this opens doors for service charge, i.e. more revenue, and faster cellular service adaptation, i.e. shutting down immediately rather than waiting for SAS orders, which depend on ESC sensors. We describe the radar detection steps as part of an O-RAN deployment in Fig. 5. The data collection happens at the BS, where I/Q samples are captured. Cellular systems in the CBRS band are required to operate in TDD mode. Hence, both UL and DL transmissions are scheduled within the band of interest. For seamless regular communication operation, we only collect spectrum data during the UL time slots, where the BS is guaranteed to be in receive mode and I/Q samples would be coming in independently of the sensing approach proposed in this paper. Notice that the O-RAN standard does not allow transmitting I/Q samples to the RICs, given that such high volumes of data could potentially saturate the interfaces. Additionally, I/Q samples contain user information, which raises privacy concerns if they are transferred outside of the BS. Therefore, SenseORAN relies uniquely upon spectrogram images, which completely resolve the privacy concern since they do not allow data decoding. Next, the spectrogram is sent to the near-RT RIC, where our custom-designed xApp runs the ML-based radar detection module. We give further details about our radar detection approach in Sec. VI. SenseORAN also supports combining multiple spectrograms for improved radar detection, which would require repeating the previous steps over time. Finally, if radar presence is detected, the xApp reconfigures the BS operation to vacate the channels where radar is detected and actively operating.

IV. SenseORAN System Model

A. Interference during Sensing and Communications

We assume a cellular deployment in the CBRS band, composed of a BS and a number of user equipments (UEs) associated with the BS. As per the FCC CBRS regulations, the cellular network works in TDD mode. Additionally, a radar transmitter may also present and the resulting radar pulses need to be sensed at the BS. The relative power level of these signals are dependent on different scenario parameters, such as distance, transmission power or noise floor, all of which impact detection accuracy. We encompass

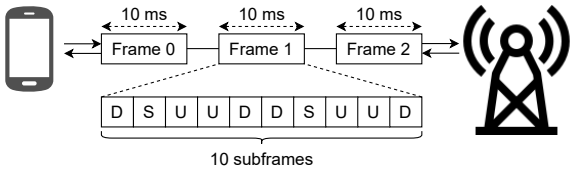

Fig. 4: TDD frame structure, where each subframe has a duration of 1 ms. An example standardized subframe configuration is shown above, where U and D represent Uplink and Downlink, respectively.

such factors by defining the peak-to-average signal-to-noise-ratio ($SINR_{sensing}$), expressed as:

$$SINR_{sensing} = \frac{P_r/B_r}{P_C/B_C + P_n/f_s} \tag{1}$$

where P_r is the radar peak power and P_C and P_n are the average cellular interference and noise powers. Additionally, B_r, B_C and f_s are the radar and cellular signal bandwidths, and the sampling rate in MHz, respectively. Notice that every term is normalized by its bandwidth and expressed in [W/MHz], given that every signal might have different bandwidths.

Next, we define $SINR_{comms}$ as the measured $SINR$ during regular cellular uplink operation, which translates into S being the UE signal and I being the interfering radar signal. We express $SINR_{comms}$ as:

$$SINR_{comms} = \frac{N_{FFT}}{T}\frac{\alpha P_C}{P_r + P_n} + \frac{T - N_{FFT}}{T}\frac{\alpha P_C}{P_n} \tag{2}$$

where T is the radar period and N_{FFT} is the 5G FFT size. α is the ratio N_{sc}/N_{FFT}, with N_{sc} as the number of subcarriers used by the cellular waveform. Notice that not every OFDM symbol will undergo radar interference. In particular, the probability of radar interference can be computed with the quotient $\frac{N_{FFT}}{T}$. Hence, Eq. 2 averages the instant $SINR$ for the symbols that will be affected by radar interference and the symbols that do not.

B. Radar Detection Using TDD Uplink Subframes

Following the assumptions above, SenseORAN only relies on UL subframes to collect sensing data. Notice that collecting inference data during the DL operation would require completely interrupting the regular communication operation, given that the BS should stop all transmissions to the associated UEs to collect the I/Q samples necessary to generate one or multiple spectrograms. Instead, UL-based sensing simply reuses the I/Q samples that are passed through the regular cellular receiver pipeline.

As we denote in Fig. 4, the number of UL and DL subframes in a TDD frame varies depending on the link configuration. For instance, 4G presents seven different subframe configurations in its TDD structure [26], expressed as $\mathcal{C}_i$, with $0 \leq i \leq 6$. Notice that the number of available UL subframes per TDD frame will impact the total time required to capture I/Q samples that are necessary to generate one spectrogram input to the xApp. We further analyze the total delay required to collect the required number of UL subframes in Sec. VIII-A.

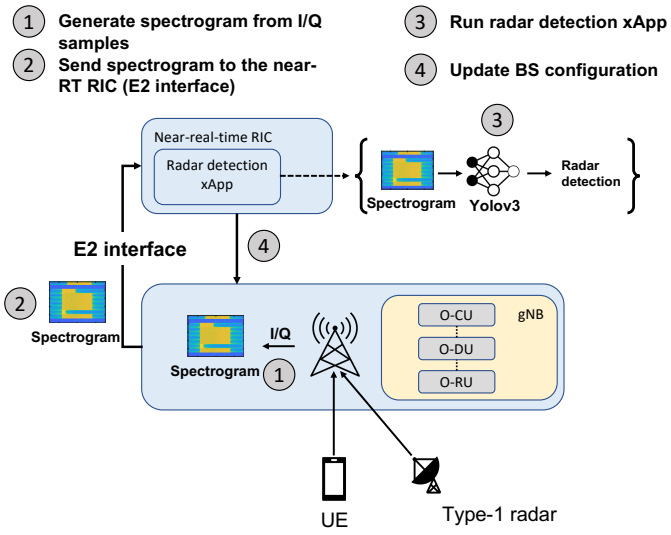

Fig. 5: The BS collects I/Q samples and generates a spectrogram image. Then, the spectrogram is sent to the near-RT RIC over the E2 interface and is used as an input to the radar detection xApp. Finally, the BS configuration is updated if an operating radar is detected.

Additionally, we note that different TDD UL subframes are concatenated to generate a single spectrogram. Given that the radar pulse repetition period is smaller than one subframe length, each subframe is guaranteed to capture one radar pulse. However, given that different UL subframes are not captured sequentially, radar pulses will look unevenly separated within the generated spectrogram. Our radar detection approach is proven to be robust to such phenomenon, as we show in Sec. VI.

C. SenseORAN System Overview

We show the overall system operation of SenseORAN in 4 steps, as depicted in Fig. 5. We describe them below:

1) Generating spectrogram from I/Q samples: I/Q samples are collected from UL subframes, as we describe in Sec. IV-B. The number of subframes is dependent on the spectrogram size and the total number of spectrograms. In this work, we fix the spectrogram length to $10\,\mathrm{ms}$. We further describe the spectrogram generation in Sec. VI-A and the impact of using multiple spectrograms in Sec. VIII. Spectograms are generated at the BS itself, to avoid sending storage-heavy I/Q samples over the E2 interface. Additionally, I/Q samples cannot leave the BS due to privacy concerns.

2) Sending spectrograms to the near-RT RIC : The E2 interface is used to share the BS-generated spectrograms with the near-RT RIC, which runs the radar detection ML models. We analyze the E2 interface latency and spectrogram overhead in Sec. VIII.

3) Running radar detection xApp: Using the spectrogram input, the presence of radar, if any, is detected by the xApp that we previously trained and deployed at the near-RT RIC. The xApp is based on state-of-the-art YOLOv3 image detection algorithm [7]. We provide further details on the radar detection approach in Sec. VI-B and its performance in Sec. VIII. Additionally, we describe the xApp implementation details in Sec. VII.

4) Update BS configuration: Upon radar detection, the xApp notifies the BS about the presence of radar over the E2 interface. Per FCC regulations, radar bands must be freed from commercial use. Accordingly, BS appropriately cuts the 5G communication in the radar operating channels.

•**Offline Model training:** In this work, the dataset is collected and radar detection model is trained offline. We provide further details for the dataset collected as well as the radar detection approach in Sec. VI. After training, the model is deployed in the near-RT RIC.

V. Preliminary Results - Radar Interference on Cellular UL Communications

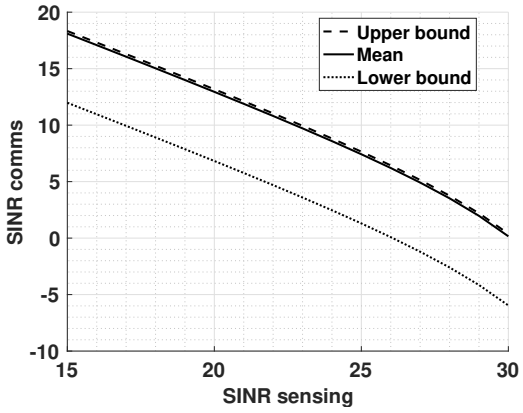

Fig. 6: Trade-off between $SINR_{sensing}$ and $SINR_{comms}$

While the primary objective of SenseORAN is to detect radar pulses overlapping with cellular signals, the former can also introduce interference on the latter. Thus, it is mutually beneficial to detect such occurrences and immediately shift cellular operation into a different band. In this preliminary study, we measure this impact quantitatively. In Fig. 6, we compare the trade-off between $SINR_{sensing}$ and $SINR_{comms}$, defined in Sec IV-A. Notice that depending on the task of interest, either radar or communication signals can act as interference (Eq. 2 and Eq. 1). Hence, the relative power levels between both signals define the accuracy of radar detection (Sec. VIII) and the quality of the cellular uplink, which we analyze in this section

Next, we set up a UL connection between a BS and a UE (Fig. 7), with simulation parameters listed in Tab. I. We simulate different modulation schemes and analyze the link performance over different SINR levels. First, we observe the $SINR_{sensing}$ range where radar is detectable, $> 12\,\mathrm{dB}$ under low traffic conditions, the link performance remains unaffected for all modulation schemes. This is partially achieved because radar signals are bursty, and multiple OFDM symbols remain interference-free. Additionally, symbol redundancy and coding rates can help recover from isolated low SINR symbols. However, as we explain in Sec. VIII-B, the $SINR_{sensing}$ levels in which radar is detectable depends on other factors,

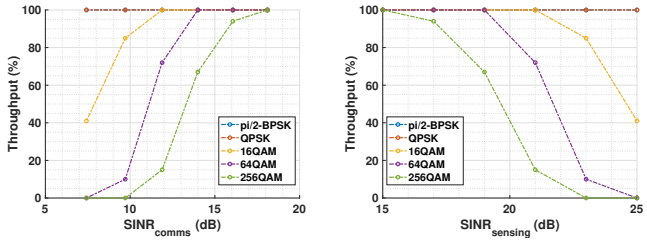

(a) (b)

Fig. 7: Percentage of max. throughput achieved versus $SINR_{comms}$ (a) and $SINR_{sensing}$ (b). Simulation specifications are detailed in Table. I.

Notation	Description	Value
B_r	Radar bandwidth	2 MHz
T	Radar period	15208 samples
T_b	Pulse length	8 samples
f_s	Sampling rate	15.36 MHz
N_{FFT}	Number of points in FFT	1024
N_{RB}	Number of resource blocks	51
B_C	Cellular waveform bandwidth	10 MHz
CP	Cyclic Prefix	Normal
SCS	Sub-carrier Spacing	15 KHz
-	Code Rate	193/1024

TABLE I: Notation Summary

such as spectrum occupancy and INR. Hence, seamless communication will not achieved under all conditions in which radar is detectable (single spectrogram detection might require $SINR_{sensing}$ up to 18 dB).

Next, we observe how radar and communication signals play the interference role, depending on the task (Eq. 2 and Eq. 1). Hence, the ratio between both signals defines the accuracy of radar detection (Sec. VIII) and the quality of the cellular uplink.

VI. Radar Detection

In this section, we describe the ML model in SenseORAN for radar detection and the dataset used for training and evaluating the performance of our model.

A. Dataset

We collect the first ever publicly accessible radar detection dataset for research purpose, consisting of overlapping over-the-air cellular and radar signals, under different noise levels and diverse traffic conditions. We use a testbed of 3 Ettus Research USRP X310 SDRs, with two nodes running a 4G cellular network and a third one to collect I/Q samples in the srsRAN's FDD mode in order to bypass the need of precisely capturing the uplink transmission moment (Fig. 8). All the SDRs are connected to the same host machine, using 10 Gbps interfaces and Ethernet cables. We setup the 4G network by running srsRAN [27], where one radio is configured as a UE and the second one as the BS. FCC defines PAL channels in the CBRS band to be 10 MHz. Here, we comply with this requirement by assigning 51 resource blocks, which requires a sampling rate of 15.36 MS/s. Additionally, we generate User Datagram Protocol (UDP) traffic at different rates between the UE and the BS. We setup an *iperf3* server at the eNB and a client on the UE side. As explained in Sec. III-C, our sensing mechanism uniquely relies on UL sub-frames. Hence, here we only capture UL transmissions. We collect a total of 1800 10 ms UL frames under 3 different traffic conditions, which capture different spectrum occupancy levels.

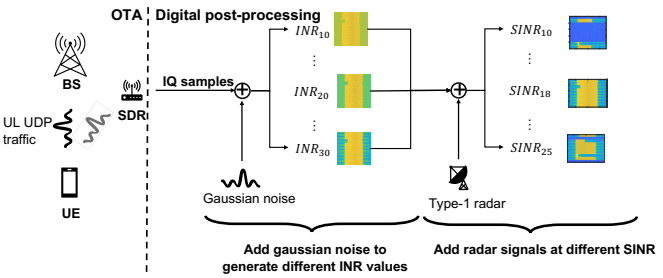

Fig. 8: Data collection pipeline

•**Spectrum occupancy:** Considering that our system achieves a maximum rate of $\sim$ 20 Mbps, we generate UDP traffic with data rates of 1 Mbps, 10 Mbps, and 30 Mbps, meaning $\sim 5\%$, 50% and 100% spectrum occupancies, respectively. Notice that traffic of 30 Mbps ensures that all resource blocks are used and guarantees full spectrum occupation. We depict examples for these three different scenarios in Fig. 10. The impact of cellular signals on radar detection ($SINR_{sensing}$) is computed following the expression in Eq. 1. Notice that this expression only considers the average interfering power over a certain band. However, interfering signals are unlikely to appear in a homogeneous manner, and may occupy the spectrum at different levels depending on the network traffic. Hence, interfering signal power distribution can exhibit considerable variance with the similar average power level (i.e. High power bursty signals versus medium power constant transmissions). How such behavior impacts radar detection, even for a fixed $SINR$ values, has not been investigated before.

•**Interference to noise ratio (*INR*):** Similar to the spectrum occupancy ratio discussed above, spectrograms with the same $SINR_{sensing}$ might will look very different depending on their *INR*s levels. In particular, high INR environments (high interference, low noise) allow the sidelobes of the radar pulses to be detectable outside of the band, where the cellular signals are present. As opposed to this, low INR translates into higher noise levels, which masks the radar sidelobes below the noise floor. The dataset was collected with an average INR of 30 dB. We extend the dataset by adding Gaussian noise, which generates the 4 extra INR values of 10 dB, 15 dB, 20 dB, and 25 dB. We exemplify the effect of different levels of *INR* on the spectrogram and radar visibility in Fig. 9.

•***SINR*$_{sensing}$ and radar parameters:** We complete the dataset generation by digitally adding standard compliant radar type-1 signals [9], with a pulse width of 8 samples, period of 15208 samples, and a sampling rate of 15.36 MS/s. We randomly assign the radar center frequency for every different spectrogram, from the range $[\frac{-B_C+B_r}{2}, \frac{B_C-B_r}{2}]$ to ensure overlapping between the radar and cellular signals. We generate spectrograms with the FFT size of 1024 and no overlap, and with $SINR$s that range from 10 dB to 25 dB for each different UDP traffic and INR value. Given the hardware requirements for FCC-

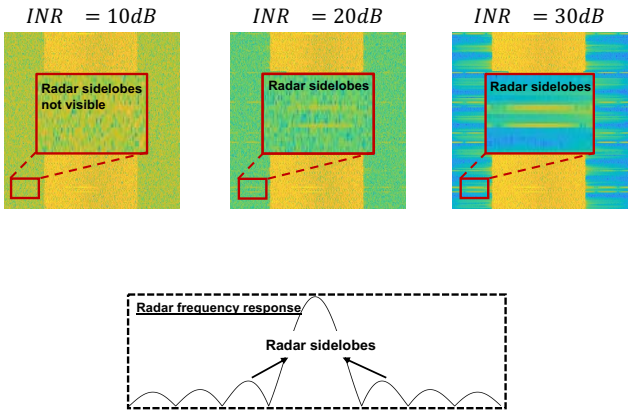

Fig. 9: Radar sidelobes are visible depending on the *INR* and/or noise floor.

compliant power levels, we neglect absolute power values and uniquely focus on relative power levels, by generating a diverse $SINR$ dataset. Notice that $SINR$ measures the relative power level between radar and interferer, which is the only representative to analyze the radar detection performance. Finally, as described in Sec. IV-B, each UL subframe will capture a radar pulse at different time instants. Hence, we generate a random delayed radar pulse for each captured UL subframe.

B. Approach

Our goal is to i) detect whether there is a radar signal present in the spectrum of interest and ii) accurately predict what frequency band the radar is operating on. To do so, we use a YOLO architecture ('you only look once'), whose speed and computational efficiency makes it one of the most popular state-of-the-art object detection algorithms [7]. In particular, similar to the work in [18], we select YOLO version 3 (YOLOv3) as it has been already proven in similar signal detection and classification problems. YOLO predicts bounding boxes for each detected object, which in this work, implies locating the radar signals in the time and frequency space of a spectrogram (see Fig. 11). While the spectrogram dataset contains both cellular and radar signals, we focus only on detecting and localizing radar transmissions. Since all 4G/5G transmissions occur with synchronization between the BS and the UEs, which frequency band and what time slots will be occupied is part of information already available within the network. Thus, our model solely focuses on detecting radar signals.

VII. Radar Detection xApp Design and Implementation in SenseORAN

In this section, we first provide an overview for the experimental setup and design of the O-RAN compliant testbed for the radar detection xApp in the near-RT RIC. Then, we detail the end-to-end implementation steps within the near-RT RIC.

A. Experimental Setup

We leverage Open AI Cellular (OAIC) platform [28], to build an LTE O-RAN system, which uses open-cellular software and software-defined radios. Specifically, the prototyped O-RAN testbed comprises of an EPC core, one LTE base station, and a varying number of UEs to establish the near-RT closed control loop. Particularly, the near-RT RIC uses E2 interface to interact with RAN. A custom E2 service model (*E2SM-SS*) is developed to send spectrogram reports and enable control of the RAN by the xApp. The near-RT RIC is deployed on a virtualized workstation based on an AMD EPYC processor, utilizing 16 CPU cores, 16 GB of RAM, and $\sim$80 GB of storage capacity. The base station and UEs are implemented in the same virtual machine and communicate to each other through ZeroMQ.

B. Implementation Workflow in the near-RT RIC

Here, we describe how the connection between the gNB and the near-RT is set up. For ease of implementation, we chose an E2-like interface based on the SCTP protocol, which functions similarly to the E2 interface and allows us to carry out control and report messages. In the E2 standard, RAN Functions define specifications and behavior of a service facilitated through the E2 interface, and are communicated by the RAN to inform the RIC of its supported capabilities. In the E2-like interface, no RAN Functions are explicitly communicated by the RAN, which initially simplifies the connection setup. There is no subscription process and no built-in differentiation of messages between E2-like nodes. Fig. 12 illustrates the workflow of our implementation, and we summarize the required steps to setup the E2-like connection below:

Step-1) The xApp is deployed, it uses the E2-like interface to accept connections from outside the RIC.

Step-2) The RAN finds the xApp and connects through the SCTP interface, establishing an E2-like connection.

Step-3) The xApp sends an acknowledgement message to the RAN which functions as a request to send *E2-Like Indication Messages*.

Step-4) Upon receiving the acknowledgement message from the xApp, the RAN starts collecting I/Q samples captured by the RF/PHY layer buffers for a specified duration. The I/Q data is reported to the xApp as an *E2-Like Indication Message*.

Step-5) The xApp receives the I/Q data and converts it into a spectrogram. In our particular implementation, spectrograms are created at the xApp itself. However, SenseORAN does not require I/Q samples to leave the BS, and this alternative was solely chosen to ease the implementation efforts. The spectrogram is fed as input to the *Spectrum Classifier*, which hosts the YOLOv3 model for radar detection. The predictions from our YOLOv3 model initiate the *Policy Controller* module.

Step-6) Then, the *Policy Controller* makes decisions based on the feedback from the YOLOv3 and issues a *E2-Like Control Message*. If the radar is detected in the band of interest, the control message dictates that all cellular operations should be terminated, as per FCC requirement in the CBRS band [29], which we comply by setting the transmitter power to near 0 W in our testbed.

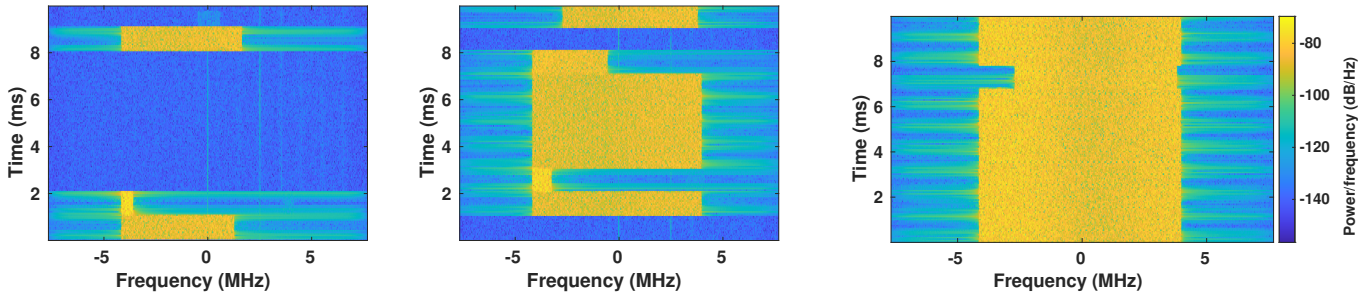

(a) (b) (c)

Fig. 10: Spectrograms with different spectrum occupancy rates of 5% (a), 50% (b) and 100% (c).

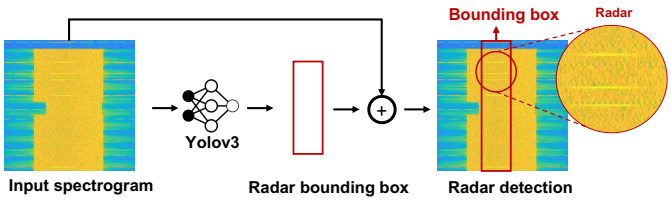

Fig. 11: YOLOv3 detects and localizes radar signals using spectrograms.

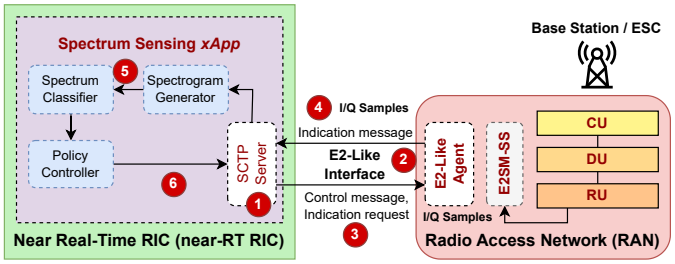

Fig. 12: Workflow for the radar detection xApp within the near-RT RIC and its interaction with the RAN.

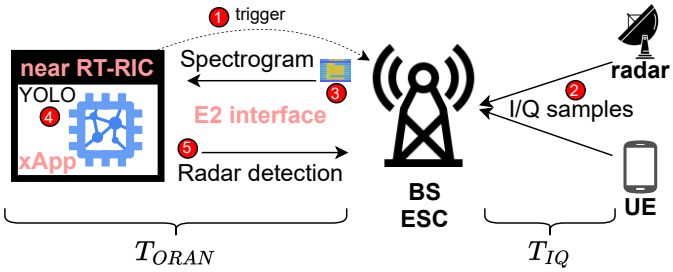

Fig. 13: Data flow and calculation steps for radar detection in an O-RAN compliant cellular network that operates in the CBRS band.

For our purposes, we implement a E2-like service model on this interface that, unlike E2, does not rely on ASN.1 for encoding and decoding of data. *E2-Like Indication Messages* from the RAN are triggered by an indication request from the xApp, unlike E2 where an event trigger may occur due to internal events such as a timer. *E2-Like Control Messages* are not required to be validated at the RAN and the success/failure is not reported back to the xApp. In order to make this system an O-RAN-compliant solution, implementing an E2 service model is required. However, our implementation works as a research proof of concept, and is conceptually the same as if a fully O-RAN compliant solution was used.

While the RU may be connected to zero or more UEs, the *E2SM-SS* service model collects I/Q samples according to the frame structure previously defined in IV-B.

VIII. Performance Evaluation

A. Time Analysis

We first study the time required to run the radar detection task when implemented within an O-RAN system. First, we identify the two main contributors to the time overhead: i) collecting I/Q samples in the time slots reserved for uplink subframes, and ii) sending the generated spectrogram image to the near-RT RIC over the E2 interface. We show where these two processes are executed in Fig. 13, and we discuss them in the remainder of this subsection.

1) Time for I/Q Sample Collection (T_{IQ}): In order to not interrupt the regular communication operation of the cellular network, we rely on I/Q samples collected during uplink time slots. Notice that the BS is already in receive mode during the period reserved for UL sub-frames. Hence, SenseORAN simply reuses I/Q samples to generate spectrograms that are otherwise being processed through the regular receiver pipeline. However, CBRS only supports TDD mode, which implies that the sensing task will be dependent on the frame configuration, as described in Sec. IV-B. The BS captures $\lambda/N_{UL}^{\mathcal{C}_i}$ frames, to complete 1 full frame of uplink I/Q data, where $\lambda = 10\,\text{ms}$ (a frame duration in TDD) and $N_{UL}^{\mathcal{C}_i}$ denotes the number of uplink subframes for the frame configuration $\mathcal{C}_i$. We express the total time needed for I/Q sample collection as:

$$T_{IQ} = \tau_{spec} \times \frac{\lambda}{N_{UL}^{\mathcal{C}_i}}, \tag{3}$$

where τ_{spec} is the time-axis duration (in s) of spectrograms created within SenseORAN. How T_{IQ} is affected by different TDD configurations is shown in Fig. 14, in which $\lambda = 10\,\text{ms}$ (default frame length in TDD, see Fig. 4). We also choose $\tau_{spec} = 10\,\text{ms}$, because we want to make the I/Q sample collection small enough to reliably detect radars and keep it consistent with the complete TDD frame duration.

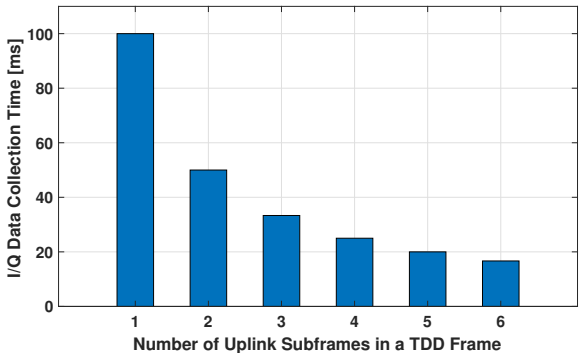

Fig. 14: The effect of TDD subframe configuration in the time it takes to collect enough I/Q samples at a BS for radar detection. For the plot above, $\tau_{spec} = 10\,\text{ms}$ and $\lambda = 10\,\text{ms}$. Note that even 1 uplink subframe is well below the upper decision time limit for an xApp in the near-RT RIC (1 s).

2) Time in the O-RAN Components (T_{ORAN}): In order to have a data flow running on the E2 interface, the end points of the interface must be connected, i.e., near RT-RIC and RAN (also called E2 nodes). E2 nodes and near RT-RIC first establish an SCTP connection, after which E2 nodes send an E2 setup request and if the near RT-RIC successfully delivers acknowledgement, then the E2 interface is setup. Since this is only required to establish a connection between the RAN and near RT-RIC, this is a one-time cost, which we denote as $T_{E2-setup}$.

After the RAN to near RT-RIC connection is established, the E2 interface is activated and the xApp is ready to function within the O-RAN network. The data flow from RAN to near-RT can occur either periodically or it might start through a trigger event by E2 nodes, whereas the data flow in the opposite direction can be initiated autonomously by the near RT-RIC or by a trigger event. We envision that the radar detection starts with a trigger from the near RT-RIC, as shown in Fig. 13. We denote the aforementioned data transmission times as $T_{RAN\rightarrow RIC}$ and $T_{RIC\rightarrow RAN}$, subtexts indicating the directions of data flow. In the $RAN \rightarrow RIC$ direction, spectrograms are sent, whereas in the $RIC \rightarrow RAN$ direction small radar detection indicators are sent. Thus, assuming that the cables in both directions in the E2 interface have identical capacity, $T_{RAN\rightarrow RIC} \gg T_{RIC\rightarrow RAN}$, making the latter practically negligible. Total data to send for a single spectrogram is $\zeta = f_s \times \sigma_{IQ} \times \tau_{spec}$, where f_s is the sampling rate (given in Tab. I), σ_{IQ} is the per sample size of the I/Q data with the value of 32 bits (16 bits for real and imaginary parts each), making $\zeta = 4.9\,\text{Mb}$. Thus, the time it takes to deliver this data over the E2 interface is $T_{E2} = T_{RAN\rightarrow RIC} = \frac{\zeta}{r_{E2}}$, where r_{E2} is the data rate (in $Mbps$) over the E2 interface.

Additionally, computations at xApps take some time. In SenseORAN, spectrograms are provided to the xApp, which detects radar pulses by applying the YOLOv3 algorithm on the spectrograms. We denote this total time as T_{RIC}, which depends on both the model complexity and ζ.

$$T_{ORAN} = T_{E2-setup} + T_{E2} + T_{RIC} \tag{4}$$

3) Complete Time for Radar Detection (T_{rd}): All in all, the total time it takes for an O-RAN compliant base-station that operates in the CBRS band is formulated as:

$$T_{rd} = T_{IQ} + T_{ORAN}, \tag{5}$$

where T_{IQ} and T_{ORAN} are provided in Eq. 3 and 4, respectively.

B. Radar Detection

In this subsection, we evaluate the performance of the radar detection approach in SenseORAN, described in Sec. VI. First, we define the following metrics:

- Recall: The ratio of true positives among all true radar labels. Notice that in radar detection, this metric is the most relevant, given that radar signals have the highest priority and the FCC mandates a radar detection of $> 99\%$ of radar pulses should be detected for an SINR of 20 dB.
- Average Intersection-over-Union (IoU): IoU for each detected radar is computed as the area of overlap of true and predicted bounding boxes, divided by the area of their union. Average IoU is calculated by averaging IoU for detected radars over the whole test set. IoU is used as a quantitative metric to measure how well the model was able to locate radar.
- Radar center frequency estimation error, defined as the absolute difference between the predicted (fc) and the ground truth (fc') center frequencies ($|fc - fc'|$).

In Fig. 15, we evaluate the performance of our model in terms of recall, average Intersection-over-Union (IoU), and radar center frequency estimation error for different *INR* and spectrum occupancy values. We observe that higher $SINR_{sensing}$ improves all 3 metrics, as expected. However, $SINR_{sensing}$ is not the only parameter that impacts the radar detection performance. While $SINR_{sensing}$ models the radar level in comparison to the interference and noise, the relative power level between these two (INR) (high interference and low noise floor), is also relevant. In Figs. 15a-15c, we analyze show how all metrics improve with higher INR values, even when the measured $SINR_{sensing}$ is the same. As explained in Sec. VI-A, even if the radar bandwidth is limited to 2 MHz, the sidelobe power dissipates beyond its allocated band. While this generates undesired interference, it can facilitate radar detection when the sidelobe power is above the noise floor. Then, in scenarios with high INR, our approach can easily detect and localize radar in a spectrogram, which translates into better recall, IoU and center frequency estimation. Next, we evaluate the impact of different spectrum occupancy patterns generated by different traffic levels. While noise is constant over time, interference will depend on many factors. However, notice that $SINR_{sensing}$ (Eq. 1) averages the interference levels for the time/frequency of interest. In Figs. 15d-15f, we show the lower the spectrum occupancy, the higher the radar detection performance. When the average level of interference and noise is the same, lower traffic/spectrum occupancy facilitates that certain radar pulses might fall into an interference-free slot

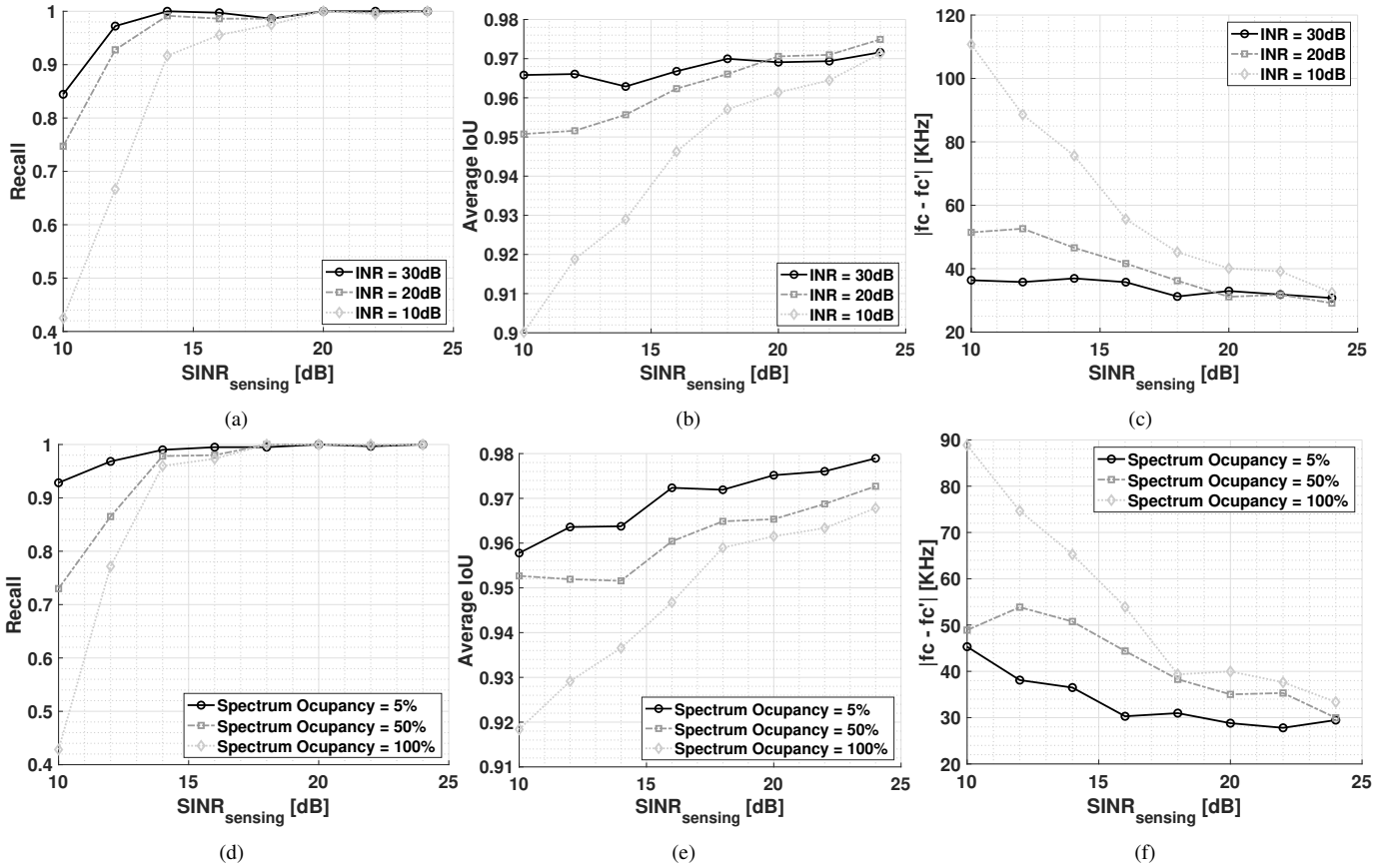

Fig. 15: Recall vs. $\text{SINR}_{\text{sensing}}$ for different *INR* (a) and spectrum occupancies (d). Average IoU vs. $\text{SINR}_{\text{sensing}}$ for different *INR* (c) and spectrum occupancies (e). fc error estimate for different *INR* (c) and spectrum occupancies (f).

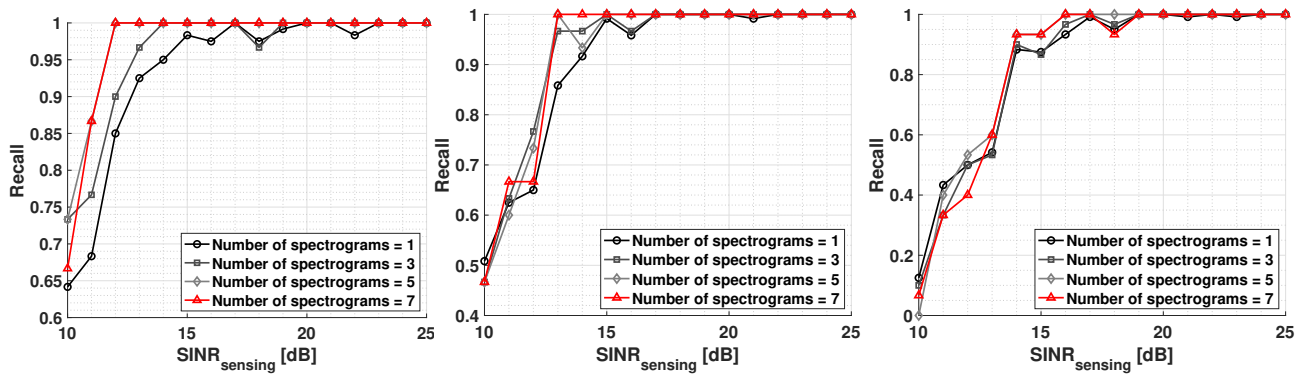

Fig. 16: Recall vs. $\text{SINR}_{\text{sensing}}$ while applying majority voting on predictions with different number of spectrograms. We compare spectrum occupancies of 5% (a), 50% (b), and 100% (c).

while completely overlapping with an ongoing transmission. Our results show that this scenario, where some radar pulses undergo *low* interference while others undergo *high* interference, is preferred over the case in which all pulses experience the same *medium* level of interference.

C. Radar Detection Using Multiple Spectrograms

The previous results always assume radar is detected using a single spectrogram. However, SenseORAN supports collecting and using multiple spectrograms to improve robustness and achieve detection at lower $SINR_{sensing}$. We evaluate the radar detection performance (recall) in Fig. 16 under different traffic conditions. All results are averaged across all *INR* values present in the dataset. When multiple spectrograms are used, each spectrogram is used to obtain an independent decision, and then all results are combined using a majority voting, which takes a final decision (radar vs no radar) based on what the majority decided. We observe how increasing the number of spectrograms improves the detection performance for all spectrum occupancy patterns, by reducing the $SINR_{sensing}$ at

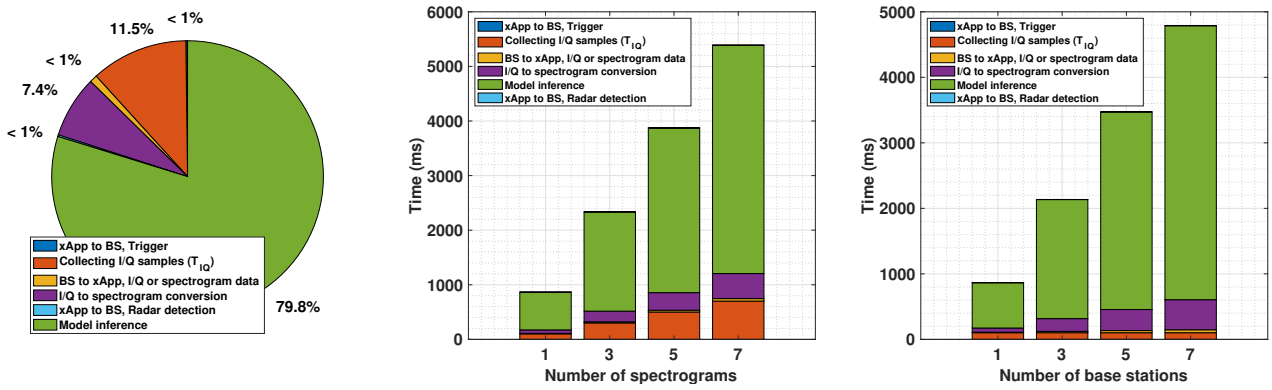

(a) (b) (c)

Fig. 17: Experimental time analysis in SenseORAN. The breakdown of the total round trip time (RTT), which is $925\,\mathrm{ms}$ (a), RTT vs. number of spectrograms (b), and RTT vs. number of base stations (c).

which the FCC required 99% detection accuracy is necessary. For instance, we achieve 100% accuracy at $12\,\mathrm{dB}$, $13\,\mathrm{dB}$, and $16\,\mathrm{dB}$ $SINR_{sensing}$. Notice that we overwhelmingly improve over the FCC thresholds in the CBRS band, which mandate at least 99% detection accuracy at $20\,\mathrm{dB}$ $SINR_{sensing}$.

D. SenseORAN System Round Trip Time

Fig. 17a presents the breakdown of overall round trip time (RTT) incurred in SenseORAN. Noticeably, the YOLOv3 model inference is the bottleneck and accounts for 79.8% of the total latency of $866\,\mathrm{ms}$ ($< 1\,\mathrm{s}$), which represents 85.5% improvement over the $60\,\mathrm{s}$ limit that is mandated by the state-of-the-art CBRS SAS system. The next two most time consuming steps take place at the BS for collecting I/Q samples over the air (T_{IQ}) and creating spectrograms from the I/Q samples, which respectively account for nearly 11.5% and 7.4% of total RTT.

Figs. 17b and 17c showcase the impact of varying number of spectrograms and number of BS over the RTT time of SenseORAN, respectively. The results are expected, as the overall effect is the overhead increase in collecting higher number of I/Q samples (multiple spectrograms from a given BS in Fig. 17b) or multiple BSs (one spectrogram per BS in Fig. 17c), and subsequent steps of I/Q to spectrogram conversion and model inference time. To evaluate the multiple BS configuration in Fig. 17c, we use the measurements for the multi-spectrogram configuration in Fig. 17b and assume that I/Q data collection happens in parallel. Finally, the E2 latency is computed accounting for the traffic overhead of supporting multiple base stations.

IX. Conclusions

We propose a novel architectural transformation within the classical cellular systems enabled by O-RAN that allows a BS to act as a spectrum sensor. In the CBRS band, SenseORAN i) eliminates the need for dedicated radar detection infrastructure, and ii) reduces the detection and system response times in comparison to the legacy CBRS-SAS approach. In addition to the reduction in cost and time, SenseORAN potentially expands the radar sensing area, given the nation-wide coverage of deployed cellular infrastructure. We demonstrate radar detection feasibility under various levels of cellular signal interference. We also analyze the practical delays and overheads using a real O-RAN system implementation with SDRs. Our results conclude a radar detection recall of $\sim 98\%$ for $SINR$s $\geq 18\,\mathrm{dB}$ under all INR and spectrum occupancy scenarios, and achieve a 100% radar detection recall for $SINR$s $\geq 12\,\mathrm{dB}$ and under low traffic conditions when 7 spectrograms are combined using majority voting. Finally, we implement our radar detection as an xApp, where we show the feasibility of SenseORAN with end-to-end response times of $< 1\,\mathrm{s}$, being compliant with the near-RT RIC O-RAN specifications and much lower than the permissible radar reporting time of $60\,\mathrm{s}$ that is mandated by the FCC.

X. Future Work

SenseORAN is the first step towards using cellular systems for both communications and sensing tasks. Here, we list the challenges and research opportunities that we plan on addressing in further development of SenseORAN:

- Hardware accelerated models: The radar detection model uses a single CPU, which we show is sufficient to achieve system response time of $1\,\mathrm{s}$. In future work, we will explore alternative hardware-optimized NN implementations to speed up the radar detection algorithm and achieve even faster end-to-end response times. For example, Wang *et al.* [30] achieves object detection run times of $< 10\,\mathrm{ms}$, by improving the ever-evolving YOLO algorithm.
- Parallelization in RIC: O-RAN RICs are expected to have multiple computing nodes tailored to run AI applications. Together with more efficient NN implementations, we will explore parallelization techniques that will enable running inference on multiple spectrograms simultaneously, given the available computation resources on demand.
- Intelligent reconfiguration: Current CBRS systems, as well as our implementation, simply forced a cellular

operator to stop transmissions after radar is detected in a given band. In future work, we will explore more intelligent solutions that exploit spectrum resources more efficiently, while guaranteeing no impact on the radar functionality.

- Extension to other sensing applications: The CBRS band coexistence problem was chosen to showcase an application, where running a sensing task as part of an xApp could be beneficial. However, we envision this concept can be extended to a wide range of problems including mobile radar in the 3.1-3.5GHz band. We will explore such alternative sensing applications, while considering real system and O-RAN implementation limitations.

ACKNOWLEDGEMENT

Authors gratefully acknowledge the funding support from the U.S. National Science Foundation (NSF) grants CNS 2112471, CNS 2229444, and CCRI 2120411 along with the Roux Institute and Harold Alfond Foundation.

REFERENCES

[1] N. N. Krishnan, R. Kumbhkar, N. B. Mandayam, I. Seskar, and S. Kompella, "Coexistence of radar and communication systems in cbrs bands through downlink power control," in *MILCOM 2017-2017 IEEE Military Communications Conference (MILCOM)*. IEEE, 2017, pp. 713–718.

[2] "An Assessment of the Near-Term Viability of Accommodating Wireless Broadband Systems in the 1675-1710 MHz, 1755-1780 MHz, 3500-3650 MHz, and 4200-4220 MHz, 4380-4400 MHz Bands," https://ntia.gov/files/ntia/publications/fasttrackevaluation_11152010.pdf, accessed: 2022-12-17.

[3] "Citizens Broadband Radio Service Device (CBSD) Types: 4G," https://www.4g-lte.net/technology/citizens-broadband-radio-service-device-cbsd-types/, accessed: 2022-12-05.

[4] "Requirements for Commercial Operation in the U.S. 3550-3700 MHz Citizens Broadband Radio Service Band," https://winnf.memberclicks.net/assets/CBRS/WINNF-TS-0112.pdf, accessed: 2022-12-05.

[5] "What Federated Wireless has learned from operating a CBRS ESC," https://www.rcrwireless.com/20200805/network-infrastructure/what-federated-wireless-has-learned-from-operating-a-cbrs-esc, accessed: 2022-12-05.

[6] "DoD Kicks Off 5G Dynamic Spectrum Sharing Experimentation at Hill AFB," https://www.defense.gov/News/Releases/Release/Article/2859222/dod-kicks-off-5g-dynamic-spectrum-sharing-experimentation-at-hill-afb/, accessed: 2022-12-17.

[7] J. Redmon and A. Farhadi, "Yolov3: An incremental improvement," *CoRR*, vol. abs/1804.02767, 2018. [Online]. Available: http://arxiv.org/abs/1804.02767

[8] L. Bonati, S. D'Oro, M. Polese, S. Basagni, and T. Melodia, "Intelligence and learning in o-ran for data-driven nextg cellular networks," *IEEE Communications Magazine*, vol. 59, no. 10, pp. 21–27, 2021.

[9] F. H. Sanders, "Procedures for laboratory testing of environmental sensing capability sensor devices," Institute for Telecommunication Sciences, Tech. Rep., 2017.

[10] "SenseORAN dataset," https://genesys-lab.org, accessed: 2023-09-10.

[11] "O-RAN testbed implementation," https://github.com/vksh224/nextg-lab.github.io, accessed: 2023-09-10.

[12] M. Polese, L. Bonati, S. D'Oro, S. Basagni, and T. Melodia, "Understanding o-ran: Architecture, interfaces, algorithms, security, and research challenges," 2022. [Online]. Available: https://arxiv.org/abs/2202.01032

[13] P. S. Upadhyaya, A. S. Abdalla, V. Marojevic, J. H. Reed, and V. K. Shah, "Prototyping next-generation o-ran research testbeds with sdrs," 2022. [Online]. Available: https://arxiv.org/abs/2205.13178

[14] D. Johnson, D. Maas, and J. K. V. der Merwe, "NexRAN: closed-loop RAN slicing in POWDER - a top-to-bottom open-source open-RAN use case," in *WiNTECH '21*, 2022.

[15] L. Bonati, S. D'Oro, S. Basagni, and T. Melodia, "Scope: An open and softwarized prototyping platform for nextg systems," in *Proceedings of the 19th Annual International Conference on Mobile Systems, Applications, and Services*, ser. MobiSys '21, 2021, p. 415–426.

[16] S. D'Oro, L. Bonati, M. Polese, and T. Melodia, "Orchestran: Network automation through orchestrated intelligence in the open ran," in *IEEE INFOCOM 2022 - IEEE Conference on Computer Communications*, 2022, pp. 270–279.

[17] M. Polese, L. Bonati, S. D'Oro, S. Basagni, and T. Melodia, "Colo-ran: Developing machine learning-based xapps for open ran closed-loop control on programmable experimental platforms," 2021. [Online]. Available: https://arxiv.org/abs/2112.09559

[18] N. Soltani, V. Chaudhary, D. Roy, and K. Chowdhury, "Finding waldo in the cbrs band: Signal detection and localization in the 3.5 ghz spectrum," in *GLOBECOM 2022-2022 IEEE Global Communications Conference*. IEEE, 2022, pp. 4570–4575.

[19] W. M. Lees, A. Wunderlich, P. J. Jeavons, P. D. Hale, and M. R. Souryal, "Deep learning classification of 3.5-ghz band spectrograms with applications to spectrum sensing," *IEEE transactions on cognitive communications and networking*, vol. 5, no. 2, pp. 224–236, 2019.

[20] R. Caromi, A. Lackpour, K. Kallas, T. Nguyen, and M. Souryal, "Deep learning for radar signal detection in the 3.5 ghz cbrs band," in *2021 IEEE International Symposium on Dynamic Spectrum Access Networks (DySPAN)*, 2021, pp. 1–8.

[21] R. Caromi and M. Souryal, "Detection of incumbent radar in the 3.5 ghz cbrs band using support vector machines," in *2019 Sensor Signal Processing for Defence Conference (SSPD)*. IEEE, 2019, pp. 1–5.

[22] S. Sarkar, M. Buddhikot, A. Baset, and S. K. Kasera, "Deepradar: A deep-learning-based environmental sensing capability sensor design for cbrs," in *Proceedings of the 27th Annual International Conference on Mobile Computing and Networking*, 2021, p. 56–68.

[23] X. Ying, M. M. Buddhikot, and S. Roy, "Sas-assisted coexistence-aware dynamic channel assignment in cbrs band," *IEEE Transactions on Wireless Communications*, vol. 17, no. 9, pp. 6307–6320, 2018.

[24] M. Grissa, A. A. Yavuz, and B. Hamdaoui, "Trustsas: A trustworthy spectrum access system for the 3.5 ghz cbrs band," in *IEEE INFOCOM 2019-IEEE Conference on Computer Communications*. IEEE, 2019, pp. 1495–1503.

[25] R. Smith, C. Freeberg, T. Machacek, and V. Ramaswamy, "An o-ran approach to spectrum sharing between commercial 5g and government satellite systems," in *MILCOM 2021-2021 IEEE Military Communications Conference (MILCOM)*. IEEE, 2021, pp. 739–744.

[26] R. Susitaival, H. Wiemann, J. Östergaard, and A. Larmo, "Internet access performance in lte tdd," in *2010 IEEE 71st Vehicular Technology Conference*. IEEE, 2010, pp. 1–5.

[27] "srsRAN - Your own mobile network," https://www.srslte.com, accessed: 2022-11-15.

[28] "Open AI Cellular," https://www.openaicellular.org, accessed: 2022-11-03.

[29] "CERTIFICATION AND TEST PROCEDURES FOR CITIZENS BROADBAND RADIO SERVICE DEVICES AUTHORIZED UNDER PART 96," https://apps.fcc.gov/kdb/GetAttachment.html?id=oXoQ1f1y7fj8yxgm424g0w\%3D\%3D&desc=940660\%20D01\%20Part\%2096\%20CBRS\%20v03&tracking_number=229297, accessed: 2023-05-30.

[30] C.-Y. Wang, A. Bochkovskiy, and H.-Y. M. Liao, "Yolov7: Trainable bag-of-freebies sets new state-of-the-art for real-time object detectors," *arXiv preprint arXiv:2207.02696*, 2022.

Guillem Reus-Muns earned his PhD in Computer Engineering from Northeastern University under Prof. Kaushik Chowdhury in 2023. Previously, he earned his B.S. in Telecommunication systems engineering from the Polytechnic University of Catalonia (UPC) and his MS in Computer Engineering from Northeastern University. His research focuses on applied AI for wireless communications, sensing, and computation. During his PhD, he interned at MathWorks, Nokia Bell Labs, and NVIDIA. In 2023, he joined Apple as a wireless systems engineer.

Pratheek S. Upadhyaya is a PhD student in the Department of Electrical and Computer Engineering at Virginia Polytechnic and State University. His research interests include radio resource management, 5G-based positioning, AI/ML applications in wireless communications, and spectrum sharing. He has contributed to the development of various 5G-based O-RAN Testbeds at Virginia Tech such as the indoor-based CORNET testbed and the outdoor-based PORT5+ testbed.

Utku Demir is an EAI Postdoctoral Research Fellow at GENESYS Lab, Department of Electrical and Computer Engineering, Northeastern University, directed by Kaushik Chowdhury. He received his PhD and M.S. degrees in electrical engineering from the University of Rochester in 2020 and 2017, respectively, working with Wendi Heinzelman. He received an M.S. and his B.S. degrees in electrical and electronics engineering from Koç University, Istanbul, in 2014 and 2012, respectively, working with Sinem Çöleri. His research interests lie in the areas of wireless communications, mobile networks, signal processing, and machine learning.

Nathan Stephenson Nathan Stephenson is an undergraduate student at George Mason University pursuing a B.S. in Computer Engineering with a minor in Music Technology. He is currently participating in a research internship with NextG Wireless Lab@Mason, focusing on software development for 5G/Next-G wireless systems involving xApps, simulations, DevOps, cybersecurity, spectrum sharing, and machine learning.

Nasim Soltani is a PhD candidate at the Department of Electrical and Computer Engineering, Northeastern University, Boston, MA. She started her PhD under supervision of Professor Kaushik Chowdhury in 2018. Her research area is ML applications for wireless systems. Her interests are within the physical layer of WiFi and cellular systems, specifically RF fingerprinting, neural network-based receiver design, signal classification, and secure communication.

Vijay K. Shah is an Assistant Professor in the Cybersecurity Engineering (CYSE) Department in the College of Engineering and Computing at George Mason University. Prior to joining Mason, he was a Research Assistant Professor at the Bradley Department of Electrical and Computer Engineering at Virginia Tech, and was affiliated with Wireless@Virginia Tech. He serves as the director for the NextG Wireless Lab@Mason, where the group focuses on the experimental research on next-generation wireless communications and networks, particularly, 5G/next-G cellular systems, open radio access networks (O-RAN), AI/ML, spectrum sharing, and wireless security.

Kaushik R. Chowdhury (M'09-SM'15) is a Professor at Northeastern University, Boston, MA. He received his Ph.D. degree from Georgia Institute of Technology in 2009. His current research interests involve systems aspects of machine learning for agile spectrum sensing/access, unmanned autonomous systems, programmable and open cellular networks, and large-scale experimental deployment of emerging wireless technologies.